JOURNAL OF SOLID STATE CHEMISTRY **141,** 365–372 (1998)
ARTICLE NO. SC987948

A New Solid Solution Series Linking $LiTi_2O_4$ and $Li_2Ti_3O_7$ Ramsdellites: A Combined X-Ray and Neutron Study

Richard K. B. Gover[1] and John T. S. Irvine[2]

School of Chemistry, University of St. Andrews, KY16 9ST Fife, Scotland

Received February 27, 1998, in revised form June 25, 1998; accepted June 25, 1998

We report the discovery of a new solid solution linking the $LiTi_2O_4$ and $Li_2Ti_3O_7$ ramsdellite phases. The solid solution system is $Li_{1+x}Ti_{2-2x}O_4$ ($0 \le x \le 0.143$), where $Li_2Ti_3O_7$ can be written as $Li_{1.143}Ti_{1.714}O_4$. Combined Rietveld refinement of X-ray and neutron diffraction data sets has been used to determine the structure of various members of this solid solution. Unit-cell dimensions were seen to decrease as the Li content increased, in accord with the expected decrease in ionic size of Ti on oxidation. The Li channel and framework occupancy was seen to follow a simple substitutional mechanism; for every two titanium atoms in the framework that are replaced by lithium atoms, one lithium is lost from the channel sites, introducing a channel vacancy site. The lithium temperature factors were seen to increase over a composition range from $x = 0$ to $x = 0.143$. This is probably related to the increased number of channel vacancies. No evidence was observed for the splitting of the Li channel sites, even for the $x = 0.143$ end member. © 1998 Academic Press

INTRODUCTION

The search for new, fast Li-ionic conductors has been area of considerable activity (1, 2), as Li-ion based systems are very attractive for battery applications due to the electropositive nature of Li and its low density. A number of lithium titanates have been investigated including Li_4TiO_4 (3), Li_2TiO_3 (4), and $Li_2Ti_3O_7$. The phase $Li_2Ti_3O_7$, which was first reported by Jonkers (5) and subsequently by Kim and Hummel (6), has a ramsdellite-type structure related to that described by Bystrom (7) for γ-MnO_2.

The crystal structure of $Li_2Ti_3O_7$ has been described as $(Li_{0.86})_c(Ti_{1.715}Li_{0.285})_fO_4$ (8, 9), with **c** and **f** indicating channel and framework sites, respectively. Abrahams *et al.* reported that Li was distributed over two sites within the channels for $Li_2Ti_3O_7$ (i.e., $Li_{1.145}Ti_{1.710}O_4$) with approximately 60% of the total Li at an 8a site (−0.058, 0.445, 0.181) and the remaining 40% at a 4*c* site (0.054, 0.047, 0.25). Morosin reported that approximately 50% Li was to be found at one 4*c* site (−0.06, 0.45, 0.25) and the remaining 50% at another 4*c* site (0.5, 0.05, 0.25). It is also well known that $Li_2Ti_3O_7$ exhibits high Li ionic conductivity, (typically 1.55×10^{-5} Scm^{-1} at 298 K) (10).

In 1994, Akimoto *et al.* (11) prepared single crystals of $LiTi_2O_4$ and deduced that the high-temperature polymorph of $LiTi_2O_4$ has a ramsdellite-type structure. This work has recently been confirmed by neutron powder diffraction (12). Both reports concluded that Li exclusively occupied a 4*c*-channel site within the structure at (−0.057, 0.45, 0.25).

The ternary phase system $Li_2O:Ti_2O_3:TiO_2$ system shown in Fig. 1 shows the location of the $LiTi_2O_4$ spinel/ramsdellite composition and its relation to the $Li_2Ti_3O_7$ ramsdellite and $Li_4Ti_5O_{12}$ spinel Ti^{IV} compositions. It is well known that the spinels $LiTi_2O_4$ and $Li_4Ti_5O_{12}$ are linked by the solid solution mechanism $Li_{1+x}Ti_{2-x}O_4$ (13), although there have been some suggestions that this system may exhibit a region of immiscibility (14). In this study, we will demonstrate that $LiTi_2O_4$ and $Li_2Ti_3O_7$ ($Li_{1.143}Ti_{1.714}O_4$) can be related to each other using the solid solution mechanism $Li_{1+x}Ti_{2-2x}O_4$.

The suggested substitution mechanism for this proposed solid solution is that for every two Ti^{3+} ions in the framework of $LiTi_2O_4$ that are replaced with lithium ions, one lithium is lost from the channel and $5Ti^{3+}$ are oxidized to Ti^{4+}. This can be expressed in Kroger-Vink notation as:

$$7Ti_f' + Li_c^x \rightarrow 2Li_f''' + 5Ti_f^x + V_c'. \qquad [I]$$

X-ray powder diffraction cannot be used to accurately determine the location of Li within the majority of structures due to its low scattering power, and neutron diffraction is usually a preferred technique. Even using neutron diffraction locating Li is not simple in lithium titanates, as the coherent scattering lengths of lithium (-2.22×10^{-24} cm^2) and titanium (-3.438×10^{-24} cm^2) mean that Ti scatters more than twice as strongly as Li (15, 16).

In the proposed model, the occupancy of Li on framework sites can be quite low and hence difficult to determine

[1]Current address: Department of Chemistry, Faculty of Science, Kobe University 1-1, Rokko-dai, Nada, Kobe, 657-8501, Japan.

[2]To whom correspondence should be addressed.

0022-4596/98 $25.00

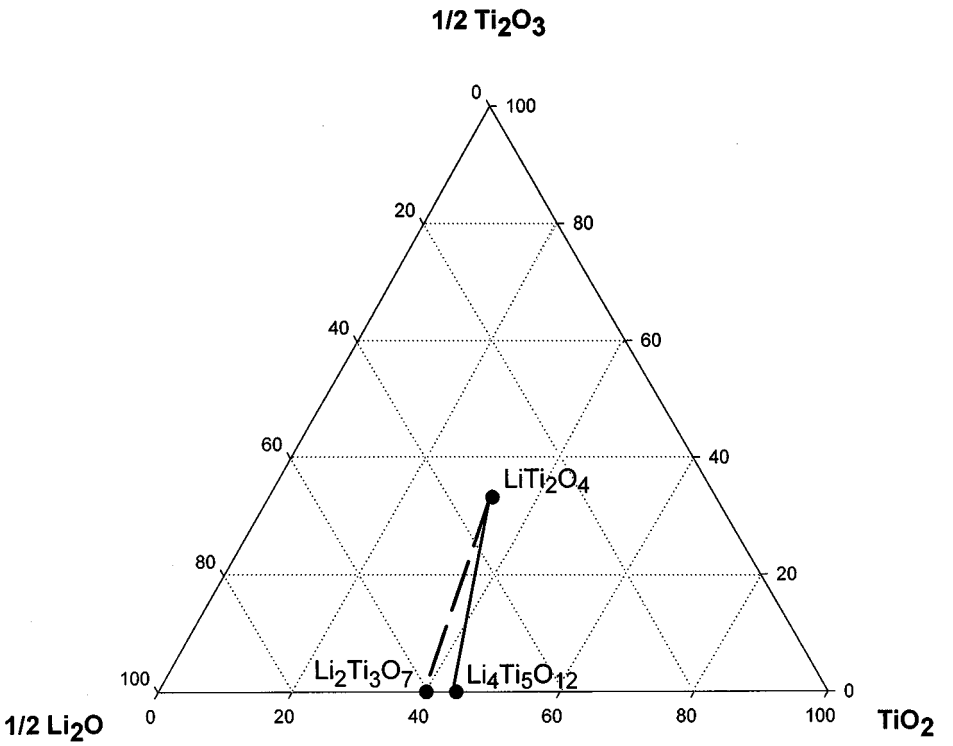

FIG. 1. $Li_2O:Ti_2O_3:TiO_2$ system (mol%) showing loci of the spinel $Li_{1+x}Ti_{2-x}O_4$ and ramsdellite $Li_{1+x}Ti_{2-2x}O_4$ solid solution systems. Note that these systems do not coexist in equilibrium at most temperatures; spinel is the stable form below 800°C and ramsdellite is the stable form above 1050°C.

from neutron diffraction. As Ti is the dominant X-ray scatterer from these sites, X-ray diffraction gives good information on the Ti occupancy. The GSAS (17) Rietveld refinement software allows the use of multiple histograms and hence data from X-ray and neutron techniques have been refined simultaneously in this study.

EXPERIMENTAL

A two-stage synthesis route was chosen involving $Li_4Ti_5O_{12}$, TiO_2 and Ti metal, using the reactions

$$2Li_2CO_3 + TiO_2 \rightarrow Li_4Ti_5O_{12} \qquad [II]$$

$$Li_4Ti_5O_{12} + 2TiO_2 + Ti \rightarrow 4Li_{1+x}Ti_{2-2x}O_4. \qquad [III]$$

The following high-purity reagents were used, Li_2CO_3 (AnalaR), Ti metal (Johnson Matthey/Aldrich), and rutile TiO_2 (Tioxide Specialities). For the preparation of the $Li_4Ti_5O_{12}$, the Li_2CO_3 and TiO_2 were predried at 500°C for at least 6 h. On drying, they were immediately weighed out in the appropriate ratios according to [II] and ground under acetone for approximately 30 min in an agate mortar and pestle. The mixture was then transferred to an alumina crucible and fired in the temperature range 680–705°C overnight to remove CO_2. This resultant mixture was pelleted in a 13-mm die at 2–3 tonnes and then refired for 3 days in a muffle furnace at 915°C to form the $Li_4Ti_5O_{12}$ spinel.

The reduced ramsdellite phases were prepared using $Li_4Ti_5O_{12}$, TiO_2, and Ti metal in the appropriate ratios as described in [III], the constituents were mixed under acetone and then pelleted using an 8-mm die at 2–3 tonnes. The pellets were then wrapped in copper foil and fired at 1000°C for 16 h under a flowing argon or argon and 5% hydrogen atmosphere. No evidence has been found to indicate that copper from the foil reacted with samples.

Compositions $x = 0$, 0.02, 0.04, 0.0715, 0.1, and 0.143 in the $Li_{1+x}Ti_{2-2x}O_4$ solid solution system were prepared. X-ray phase purity was determined using a Philips PW1170 diffractometer using Cu$K\alpha$ (radiation), or a Stoe Stadi P transmission diffractometer, using Cu$K\alpha_1$ radiation. The unit cells of all members of the proposed solid solution series were initially indexed using the STOE computer program LATREF (18). Thermal analysis was performed to check stoichiometry using a TA Instruments 2960 connected to a personal computer. The samples were heated at 10°C/min to 400°C and then held isothermally for 1 h in a flowing oxygen atmosphere, with a flow rate of 75 ml/min. These conditions were found to provide the most accurate

determinations of oxygen content, indeed using higher temperatures, e.g., 500°C can lead to lithia loss.

Rietveld analysis was performed on data collected on a Stoe Stadi X-ray transmission diffractometer and the neutron General Purpose Powder Diffractometer (GPPD) at the IPNS facility, located at Argonne National Laboratory, Illinois. Each X-ray data set was collected for at least 14 h in the 2θ range 15–85°, and the neutron data sets were collected for 16–20 h with refinements being performed using the 148° backscattering bank. Rietveld refinement of data was performed using the GSAS software package (Von Dreele and Larson, University of California, 1995) running on a personal computer.

TABLE 1
Unit-Cell Edge versus Composition for $Li_{1+x}Ti_{2-x}O_4$ Solid Solution as Determined from X-Ray Powder Diffraction

X composition	*a*	*b*	*c*
0	5.0356(1)	9.6394(2)	2.9464(5)
0.04	5.0315(6)	9.6235(1)	2.9486(4)
0.0715	5.0215(3)	9.5924(5)	2.9490(1)
0.1	5.0225(1)	9.5912(3)	2.9490(8)
0.143	5.0202(2)	9.5570(4)	2.9473(1)

RESULTS

All samples prepared in this solid solution series were seen to have very similar X-ray patterns, with high phase purity observed for all compositions prepared. It was possible to index the X-ray diffraction patterns of all of the samples in the proposed solid solution series as being primitive orthorhombic. Least-squares fitting of the unit cells indicated a gradual decrease in the unit-cell dimensions as a function of increasing lithium content in (see Table 1). The unit-cell dimensions obtained for this solid solution series are in good agreement with those reported previously for both $Li_2Ti_3O_7$ (8, 9) and $LiTi_2O_4$ (11). A refined X-ray powder diffraction pattern for $Li_{1.1}Ti_{1.8}O_4$ is presented in Fig. 2. As can be seen from the pattern, the sample is of high phase purity and good crystallinity. The two extra peaks found at approximately 21.4 and 23.8° 2θ, are due to a small impurity (?ZnO) in the petroleum jelly used for sample mounting.

Samples were also examined using thermogravimetric analysis (TGA) to confirm stoichiometry. Samples with Ti oxidation states less than 4 were heated to 400°C under flowing oxygen and the observed weight increase was used to determine initial stoichiometry. Oxidation commenced between 150 and 200°C, with the rate of oxidation rapidly increasing as the samples were heated from 300 to 400°C. A typical thermal analysis result is shown in Fig. 3a, and results from these thermogravimetric experiments are summarized in Fig. 3b. The determined Ti-oxidation states for most samples were in good agreement with the value expected from their nominal starting composition, confirming the proposed solid-solution mechanism. The slight

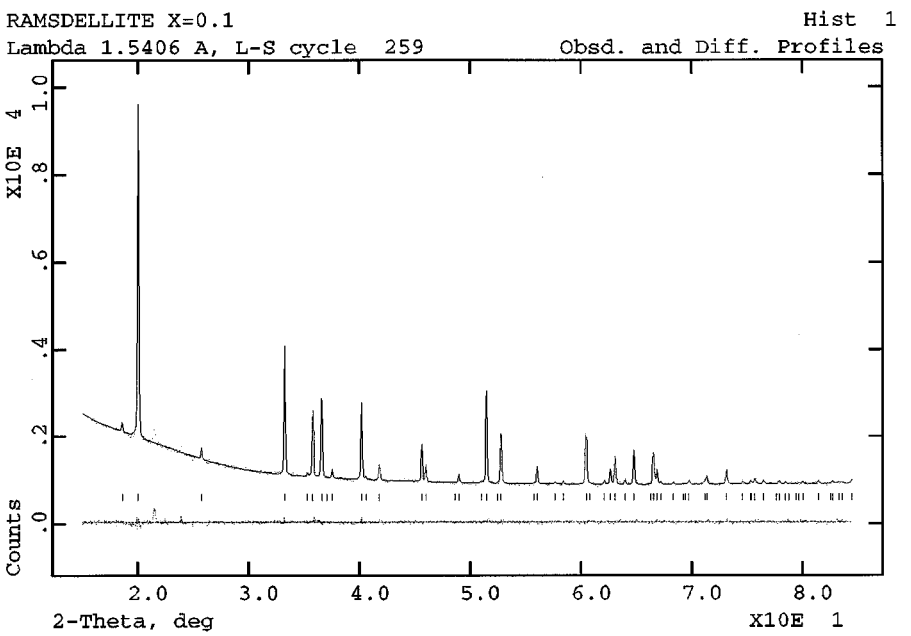

FIG. 2. Refined X-ray powder pattern obtained for $Li_{1.1}Ti_{1.8}O_4$ ramsdellite. Experimental data presented as points, calculated profile presented as a line, and the observed difference profile is plotted along the bottom.

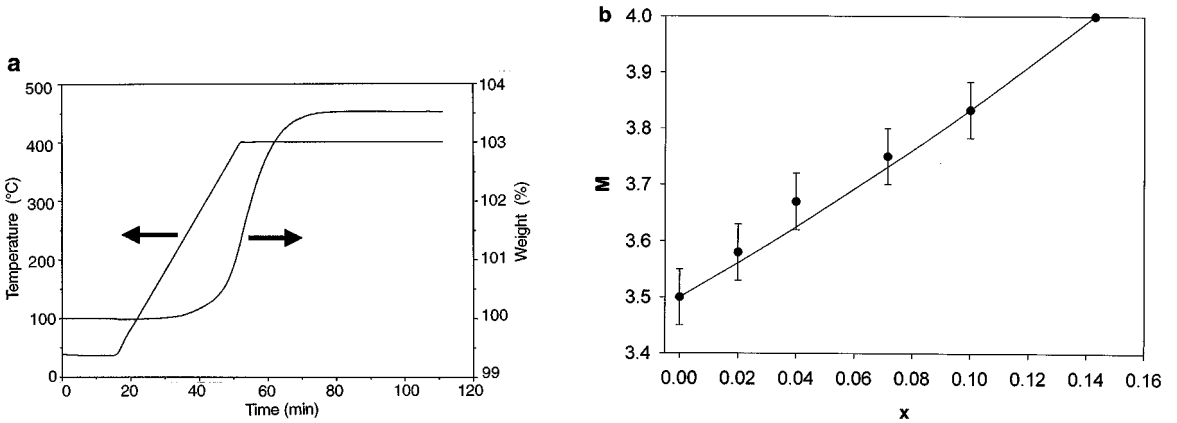

FIG. 3. (a) Typical TGA plot showing oxidation of $Li_{1.02}Ti_{1.94}O_4$. (b) Comparison of Ti oxidation state (M) determined by thermogravimetry and that calculated from initial composition in the system $Li_{1+x}Ti^{M+}_{2-2x}O_4$.

variation observed in samples such as $Li_{1.04}Ti_{1.92}O_4$ is not surprising due to the facility of oxidation. If samples oxidize at 150°C under the dynamic conditions used in thermogravimetry, slight oxidation might be anticipated on handling powders under ambient aerobic conditions prior to the thermogravimetric experiment.

The basic model used in the refinement of all members of the solid-solution series was as described previously for $LiTi_2O_4$ (12) using the *Pbnm* space group with only one (4*c*) channel site being occupied. Initial refinements were performed using X-ray data sets only and no attempt was made to refine the Li position or temperature factors, due to the low X-ray scattering factors of this element. It was also found impossible to reliably refine the temperature factors of Ti, O1, and O2.

The structural data obtained from the X-ray data were used as the starting point for the combined neutron and X-ray powder diffraction refinements. The values of the neutron scattering cross sections used during the refinement of the neutron powder patterns are presented in Table 2. As can be seen from the typical refined powder patterns presented in Fig. 4, good refinements were obtained and the samples were of high phase purity. The obtained *R* factors are presented in Table 3. Atomic positions, site occupancies, and temperature factors are presented in Tables 4 and 5, with selected bond angles and lengths presented in Table 6.

TABLE 2
Neutron Cross Sections for Lithium, Titanium, and Oxygen

Element	Coherent neutron scattering cross section
Li	−0.22220
Ti	−0.35580
0	0.58050

Examination of the neutron patterns and the error values indicates that the proposed model is correct, although the data for $x = 0.0715$ are not quite as good as that for the others, due to the presence of a slight second phase.

The unit-cell edges obtained from refinement of the combined X-ray and neutron data sets are presented in Fig. 5. These are plotted so that the percentage change in each axis is on a similar scale. The **b** axis, which relates to the longer cross-channel direction, is clearly the most sensitive to extent of substitution. The **a** unit-cell edge also decreases as Ti oxidation state increases; however, **c**, which is parallel to the channels, is essentially invariant with composition.

All samples refined satisfactorily to a simple model with one framework cation 4*c* site occupied by Ti/Li and one channel cation 4*c* site occupied by Li and vacancies. The total framework site occupancy was allowed to vary; however, its value always remained very close to one, thus indicating that no framework vacancies were present in these samples. Additional channel sites have been suggested to be occupied by Li in $Li_2Ti_3O_7$ by both Morosin and Mikellsen (8) and Abrahams *et al.* (9); Grins and West (19) have also proposed several other possible Li sites within the

TABLE 3
Residual Factors Obtained during Refinements of Combined X-Ray and Neutron Data Sets

	R_{wp} (N)	R_{wp} (X)	R_{wp} (C)	R_p (N)	R_p (X)	R_p (C)	χ^2
0	5.24	3.31	4.44	3.34	2.18	2.87	2.636
0.04	6.13	3.27	5.08	3.27	2.34	3.39	2.263
0.0715	6.71	4.84	3.19	4.46	3.19	3.92	3.586
0.1	5.05	3.37	4.24	3.27	2.15	2.74	1.820
0.143	6.06	3.79	5.10	3.83	2.55	3.29	2.680

Note. $\chi^2 = [R_{wp}(C)/R_E(C)]^2$. *N*, Neutron; *X*, X-ray; *C*, Combined.

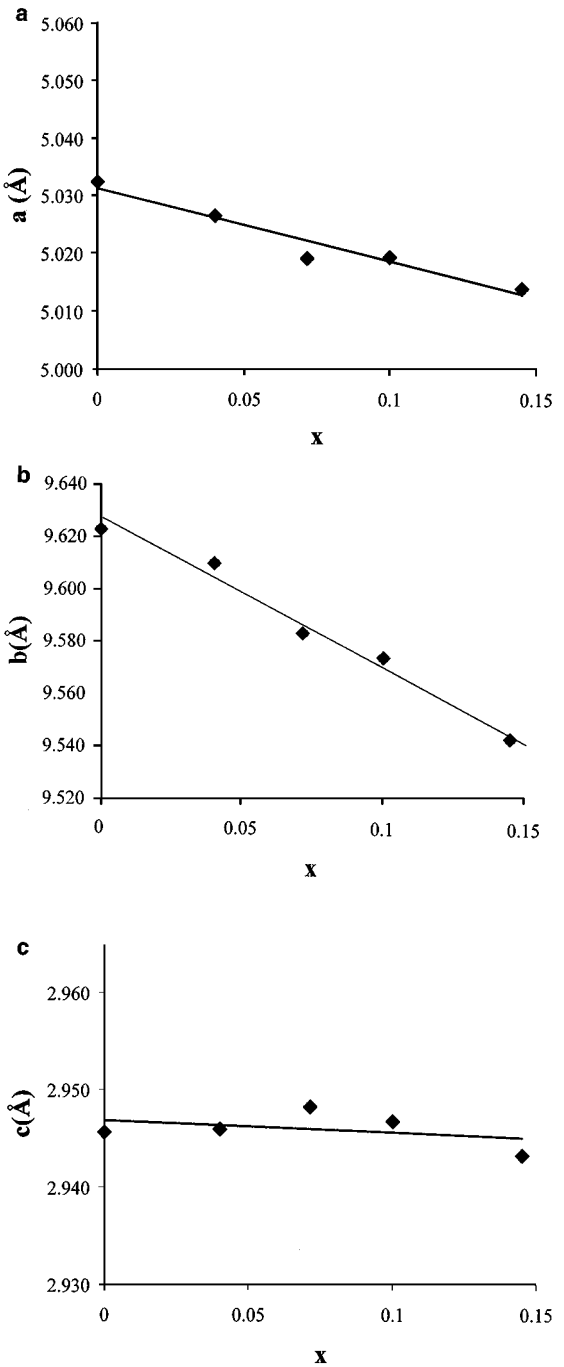

FIG. 4. Unit-cell edges versus composition as determined from refinement of combined X-ray and neutron diffraction data.Lines of best fit used as guides to the eye.

channels of the ramsdellite structure for the $Li_{2+x}(Li_xMg_{1-x}Sn_3)O_8$ $(0 \le x \le 0.5)$ and $Li_2Mg_{1-x}Fe_{2x}Sn_{3-x}O_8$ $(0 \le x \le 1)$ analogues. Several attempts were made to test for such additional channel sites both by direct refinement and by Fourier difference mapping; however, these extra sites were found to be unoccupied at room temperature for samples prepared under the slow-cooling regime used in this study.

TABLE 4
Obtained Atomic Positions and Site Occupancies for the $Li_{1-x}Ti_{2-x}O_4$ Solid Solution Series as a Function of x

	0	0.04	0.0715	0.1	0.143
			Li(1)		
x	−0.0559(2)	−0.0598(2)	−0.0580(4)	−0.0605(2)	−0.0629(2)
y	0.4687(2)	0.4675(2)	0.4411(3)	0.4752(3)	0.4581(3)
SOF	0.47(1)	0.479(1)	0.416(3)	0.432(1)	0.425(1)
			Ti/Li(2)		
x	−0.0177(3)	−0.0196(3)	−0.0248(5)	−0.0247(3)	−0.0327(3)
y	0.1416(2)	0.1416(2)	0.1401(3)	0.1409(1)	0.1407(2)
SOF	1	0.943(4)/ 0.063(7)	0.913(6)/ 0.084(12)	0.893(3)/ 0.124(7)	0.837(4)/ 0.111(8)
			O(1)		
x	0.6987(2)	0.6953(2)	0.6851(4)	0.6851(2)	0.6721(2)
y	0.2794(1)	0.2765(1)	0.2754(2)	0.2765(1)	0.2738(9)
SOF	1	1	1	1	1
			O(2)		
x	0.2022(2)	0.2031(2)	0.2031(3)	0.2027(2)	0.2042(2)
y	−0.0354(1)	−0.03531(9)	−0.0347(2)	−0.0342(9)	−0.0322(8)
SOF	1	1	1	1	1

Note. S.O.F. is an abbreviation for site occupancy factor.

TABLE 5
Temperature Factors for $Li_{1+x}Ti_{2-2x}O_4$ as a Function of Composition

	0	0.04	0.0715	0.1	0.145
			Li(1)		
$u11$	3.5(5)	1.67(43)	—	1.61(41)	—
$u22$	19.3(14)	27.9(24)	—	34.8(28)	—
$u33$	4.2(5)	8.22(87)	—	4.83(69)	—
$u12$	3.0(7)	1.35(76)	—	1.71(84)	—
UI_1	6.89(25)	7.60(30)	9.47(75)	7.76(31)	7.45(36)
uI_2	9.01	9.38	—	13.72	—
			Ti(Li2)		
$u11$	1.44(7)	1.37(7)	1.44(1)	1.50(7)	1.60(8)
$u22$	0.72(6)	0.92(6)	1.70(1)	0.78(6)	1.16(7)
$u33$	0.60(5)	0.46(5)	0.82(9)	0.99(5)	0.83(6)
$u12$	0.12(6)	0.24(6)	0.13(1)	0.11(5)	0.53(6)
			O(1)		
$u11$	1.20(4)	1.32(4)	2.04(9)	1.49(4)	1.74(5)
$u22$	1.63(6)	1.62(6)	1.79(9)	1.31(5)	1.43(5)
$u33$	0.68(5)	0.60(5)	0.23(7)	0.86(5)	0.71(5)
$u12$	0.74(5)	0.73(5)	0.85(8)	0.60(4)	0.74(4)
			O(2)		
$u11$	0.83(3)	0.78(4)	0.86(6)	0.75(3)	0.78(4)
$u22$	0.95(5)	1.13(5)	1.53(9)	0.97(4)	1.20(5)
$u33$	0.70(6)	0.96(5)	1.09(9)	0.90(5)	1.48(5)
$u12$	−0.04(4)	−0.16(4)	−0.14(8)	0.00(4)	0.04(4)

Note. UI_1 is the isotropic temperature factor obtained by direct refinement, UI_2 is the isotropic temperature factor calculated indirectly from refinement with anisotropic Li temperature factors.

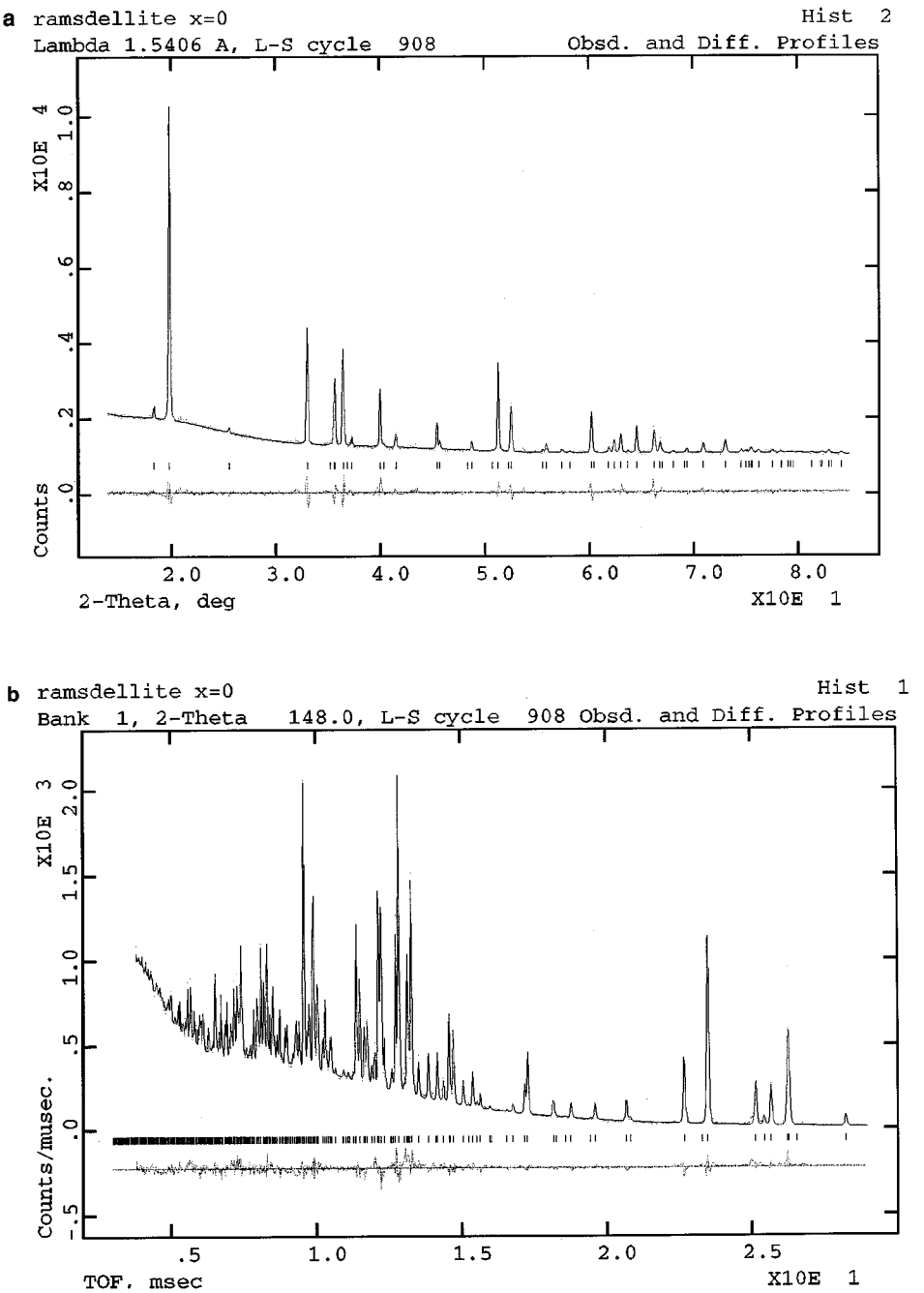

FIG. 5. Refined X-ray (a) and neutron powder diffraction (b) patterns obtained for $LiTi_2O_4$ ramsdellite. Experimental data are presented as points and the calculated profile is presented as a line.Along the bottom is the observed difference profile.

It was not possible to successfully refine the temperature factors for $x = 0.0715$ and 0.145 anisotropically. In the case of $Li_{1.0715}Ti_{1.857}O_4$, it is thought that the presence of a slight impurity was responsible for instability of the refinement of the Li anisotropic temperature factors. Abrahams *et al.* (9) also found it impossible to refine the anisotropic temperature factors for Li on the 4*c*-channel site in $Li_2Ti_3O_7$ ramsdellite. To make it possible to compare the temperature factors for all of the solid solution series, all members of the series have an isotropic temperature factor quoted for Li1. These values were obtained both directly from an isotropic refinement and indirectly, being calculated from anisotropic values using the BIJCALC routine contained in GSAS. The value obtained for uI_1 is for

TABLE 6

Selected Bond Angles and Lengths Obtained from Combined X-ray and Neutron Data Sets for $Li_{1+x}Ti_{2-2x}O_4$ Solid Solution Series

	0	0.04	0.0715	0.1	0.145
Li–O1	2.239 (11)	2.225(13)	2.053(25)	2.220(13)	2.132(13)
Li–O2	1.792(10)	1.771(12)	1.785(21)	1.767(12)	1.784(12)
Li–O2′ × 2	2.010(7)	2.015(8)	2.104(2)	2.031(8)	2.072(8)
Mean	2.011	2.007	2.012	2.012	2.015
Li–Li	1.688(7)	1.709(4)	1.945(2)	1.662(1)	1.788(2)
Ti–O1	1.952(2)	1.954(2)	1.955(3)	1.957(2)	1.955(2)
Ti–O1′ × 2	1.979(1)	1.971(1)	1.979(2)	1.970(1)	1.969(1)
Ti–O2 × 2	2.020(1)	2.020(1)	2.004(3)	2.004(1)	1.997(1)
Ti–O2′	2.032(1)	2.035(2)	2.025(3)	2.026(1)	2.029(1)
Mean	1.997	1.995	1.996	1.989	1.986
			Angles		
O2–Li–O2′	128.3(3)	128.0(4)	136.8(3)	126.8(4)	122.0(5)
O2′–Li–O2′	94.8(4)	94.0(5)	94.1(9)	93.0(5)	90.5(5)
O2–Li–O1	120.6(6)	122.8(7)	120.9(9)	126.7(7)	136.5(1)
O2–Li–O1	85.4(4)	85.1(4)	88.4(2)	85.0(4)	86.3(1)
O1–Ti–O1′	98.16(5)	98.18(5)	97.20(9)	97.59(5)	97.23(6)
O1–Ti–O2	90.16(6)	90.10(2)	89.92(1)	90.20(6)	90.58(6)
O1–Ti–O2′	165.40(9)	165.24(9)	165.78(2)	165.53(8)	166.11(9)
O1–Ti–O1	96.19(8)	96.75(9)	96.28(1)	96.79(8)	96.80(8)
O1–Ti–O2′	91.56(6)	91.58(6)	92.27(1)	91.99(5)	91.97(6)
O1′–Ti–O2	84.46(3)	84.19 (3)	84.04(4)	83.75(3)	83.55(3)
O2–Ti–O2	93.65(7)	93.62(8)	94.73(2)	94.62(7)	92.01(8)

refinement with isotropic temperature factors, whereas uI_2 is the equivalent isotropic temperature factor calculated from anisotropic values. Note that all thermal parameters are multiplied by 100.

CONCLUSIONS

Both structural and thermogravimetric studies confirm the successful preparation of this new solid solution series $Li_{1+x}Ti_{2-x}O_4$. The crystal structures of both Li_2Ti_3O7 (8, 9) and $LiTi_2O_4$ (11) have been reported previously in the literature, and it was found that the unit cells obtained from our studies are in good agreement with these values. As the Li content of the solid solution increased it was seen that the *a* and *b* edges of the unit cell decreased in magnitude, which is consistent with the overall titanium oxidation state increasing from 3.5+ toward 4+. The *c* axis was relatively insensitive to the Li content. This lack of sensitivity of the *c* axis to the composition has been seen previously by Thackerkay *et al.* while working on MnO_2 ramsdellite (20), by Akimoto *et al.* working on topotactic oxidation of $LiTi_2O_4$ (21), and by Lacorre *et al.* (22) working on $Li_{1+x}(Li_{2x/3}Fe_{1-x}Sn_{1+x/3})O_4$ ramsdellites ($0 \leq x \leq 0.28$).

The positions of both framework and channel atoms within the unit cell do not vary significantly across the solid solution series. The site occupancy of Li in the channel sites refined to 0.47 for $LiTi_2O_4$, essentially in accord with the chemical formula. From $x = 0.04$ to 0.0143, the general trend is for the total channel occupancy to decrease with increasing total Li content. The decreasing Li content within the channel as *x* increases was as expected and approximately matches that expected from the proposed model (see Fig. 6).

It must be noted that it was not possible to refine either of the two channel site models proposed by Abrahams *et al.* (9) and Morosin and Mikellsen (8), which were discussed in the Introduction. A possible explanation for the differences in

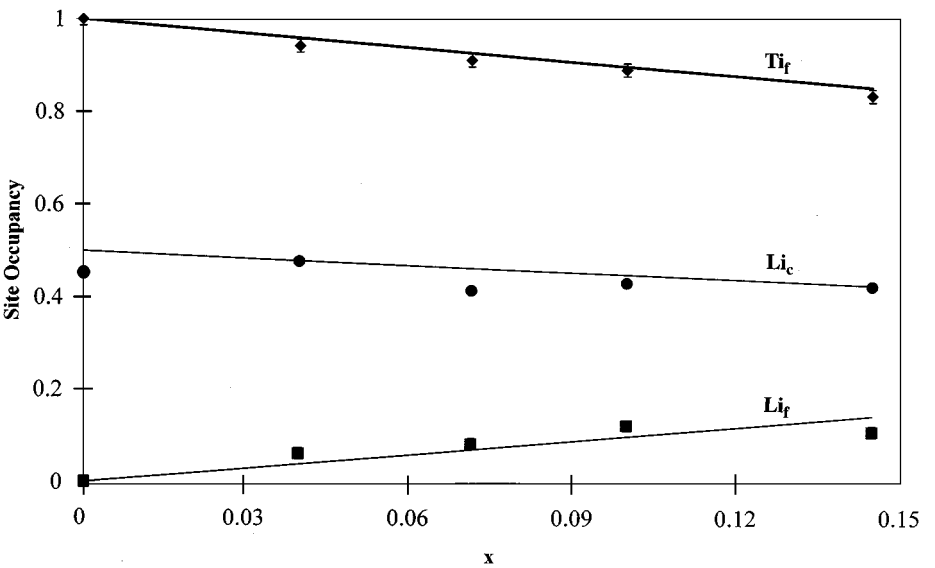

FIG. 6. Observed cation site occupancies from combined X-ray and neutron powder diffraction, compared to expected occupancies for $[Li_{1-2x}]_c[Li_xTi_{2x}]_fO_4$; *c*, channel site; *f*, framework site.

the results may be related to thermal history as the samples prepared for this study were slow cooled, whereas those of previous studies were air quenched (9). It should be noted that the structural model proposed in this study is consistent across the entire solid solution mechanism and is in accord with that proposed for $LiTi_2O_4$ ramsdellite (11, 12), whereas the models with excess Li atoms on the channel sites relate only to $Li_2Ti_3O_7$ ramsdellite.

The temperature factors obtained for the Li channel sites were high, consistent with the expected mobility of Li ions within the channels. Isotropic temperature factors were fairly constant across the series; however, the dominant anisotropic component, u_{22} increased strongly with x. This increase with x is associated with the increase in Li channel vacancies. The Ti (and Li_f), O1 and O2 temperature factors have typical values for a complex oxide and are fairly constant across the solid solution series.

The mean Li–O bond length is unchanged across the solid solution series; however, the mean Ti(Li_f)–O bond length decreases as the Ti oxidation state and the degree of Li occupation of the framework site increases.

ACKNOWLEDGMENTS

R.K.B.G. acknowledges the Russell Trust for funding a visit to IPNS to collect data and the University of St. Andrews for the provision of a studentship. We also thank Russell Morris and Susan Blake for their advice on Rietveld refinement, and Ray Thomas for his assistance with data collection. J.T.S.I. acknowledges the Nuffield Foundation for the provision of a Science Research Fellowship. This work has benefited from the use of the Intense Pulsed Neutron source at Argonne National Laboratory. This facility is funded by the U.S. Department of Energy, BES-Materials Science, under Contract W-31-109-ENG-38.

REFERENCES

1. H. Y. P. Hong, *Mater. Res. Bull.* **13,** 117 (1978).
2. I. Abrahams, P. G. Bruce, W. I. F. David, and A. R. West, *J. Solid State Chem.* **75,** 390 (1988).
3. B. L. Dubey and A. R. West, *Nature Phys. Sci.* **235,** 155 (1972).
4. M. Castellanos and A. R. West, *J. Mater Sci.* **14,** 450 (1979).
5. G. H. Jonkers, in "Trabojos Reunion Intern Reactividad Solidos," p. 413, Madrid, 1957.
6. K. H. Kim and F. A. Hummel, *J Am. Ceram. Soc.* **43,** 611 (1960).
7. A. M. Bystrom, *Acta Chem. Scand.* **3,** 163 (1949).
8. B. Morosin and J. C. Mikellsen Jr, *Acta Crystallogr. B* **35,** 798 (1979).
9. I. Abrahams, P. G. Bruce, W. I. F. David, and A. R. West, *J. Solid State Chem.* **78,** 170 (1989).
10. J. B. Boyce and J. C. Mikkelsen Jr, *Solid State Comm.* **31,** 741 (1979).
11. J. Akimoto, Y Gotoh, M. Sohma, K. Kawaguchi, Y. Oosawa, and H. Takei, *J. Solid State Chem.* **110,** 150 (1994).
12. K. B. Richard, J. Gover, T. S. Irvine, and A. A. Finch, *J. Solid State Chem.* **132,** 382 (1997).
13. A. Desanvres, B. Raveau, and Z. Sekkal, *Mat. Res. Bull.* **15,** 699 (1969).
14. M. R. Harrison, P. P. Edwards, and J. B. Goodenough, *Phil. Mag.* **52,** 679 (1985).
15. V. F Sears, *Neutron News* **3,** 29 (1992).
16. G. E. Bacon, "Neutron Diffraction," p. 21, Oxford Univ. Press, London, 1962.
17. A. C. Larsen and R. B. Von Dreele, *Los Alamos Laboratory Report*, NO-LA-U-86-748 (1987).
18. "STOE Stadi P User Guide," Stoe Automated diffractometer systems for powder and single crystal diffractometry, Darmstadt, 1987.
19. J. Grins and A. R. West, *J. Solid State Chem.* **65,** 265 (1986).
20. M. M. Thackeray, M. H. Rossouw, R. J. Gummow, D. C. Liles, L. Perce, A. De Kock, W. I. F. David, and S. Hull, *Electrochim. Acta* **9,** 1259 (1993).
21. J. Akimoto, Y. Gotoh, Y. Oosawa, N. Nonose, T. Kumaghi, K. Aoki, and H. Takei, *J. Solid State Chem.* **113,** 27 (1994).
22. P. H. Lacorre, M. Hervieu, J. Pannetier, J. Choisnet, and B. Raveau, *J. Solid State Chem.* **50,** 196 (1983).